Available online at www.sciencedirect.com
SCIENCE DIRECT®
Journal of Solid State Chemistry 177 (2004) 457–460
JOURNAL OF SOLID STATE CHEMISTRY
http://elsevier.com/locate/jssc

Effect of boron non-stoichiometry on *B*-site in perovskite type structure ScB_xRh_3 and CeB_xRh_3 on charges of atoms on *A*-site: study by X-ray photoelectron and nuclear magnetic resonance spectroscopies

Masaoki Oku,* Toetsu Shishido, Takeshi Shinohara, Qiang Sun, Yoshiyuki Kawazoe, Kazuo Nakajima, and Kazuaki Wagatsuma

Institute for Materials Research, Tohoku University, 2-1-1 Katahira, Sendai 980-8577, Japan

Received 2 July 2002; accepted 24 March 2003

Abstract

The solid solutions of $ScBRh_3$–$ScRh_3$ and $CeBRh_3$–$CeRh_3$ are synthesized by the arc melting method, where $RBRh_3$ and RRh_3 (R = rare earth element) have perovskite and $AuCu_3$ type structures, respectively. The binding energy of Sc $2p_{3/2}$ for ScB_xRh_3 increases with the boron concentration. The Knight shift of ^{45}Sc observed by nuclear magnetic resonance spectroscopy decreases with increase of boron concentration. The decrement of the Knight shift corresponds the Sc 4*s* electron density at the Fermi level. The intensity ratio of f^2:f^1:f^0 of Ce 3*d* XPS spectrum changes with boron concentration of CeB_xRh_3. It is concluded that in both cases of ScB_xRh_3 and CeB_xRh_3 the charge on the atoms on *A*-site changes with the concentration of the atoms on *B*-site, where the atoms are not directly bound.

Keywords: Perovskite type structure borides; Non-stoichiometry on *B*-site; Charge of atoms on *A*-site; ScB_xRh_3; CeB_xRh_3

1. Introduction

Metal borides have been studied to obtain superconductors and mechanically hard compounds. The authors have explored new properties of *R*–B–Rh (*R* = Sc, Y, and La) systems; in which $RBRh_3$ have perovskite type structures. We found $ScBRh_3$ [1] and $CeBRh_3$ [2] have solid solutions with $ScRh_3$ and $CeRh_3$, respectively, where the latter compounds have ordered $AuCu_3$ type structures. The schematic crystal structures of perovskite and ordered $AuCu_3$ type compounds are shown in Fig. 1. In perovskite type structure, Sc (or Ce) and boron atoms are on *A*- and *B*-sites, respectively. Rh atoms are on face center sites. The solid solution in the $ScBRh_3$–$ScRh_3$ and $CeBRh_3$–$CeRh_3$ means that the systems have non-stoichiometry on *B*-site in perovskite type structure. Generally, the non-stoichiometry in perovskite oxides is observed in deficient of oxygen atoms on the face center sites. Another factor of change of the properties is the substitution of the atoms on *A*- or *B*-sites. The deficiency of atoms on *A*- and *B*-sites have been found in rare cases such as $Ba_{1-x}U_{1-x}O_3$ [3] and $La_{1-x}Mn_{1-x}O_3$ [4]. Other systems are the *A*-site deficient perovskite oxides with the general formula $A^{4+}_{0.25}\square_{0.75}B^{5+}O_3$ (A = Ce, Th, U; B = Nb, Ta; $\square$ = vacancy) [5]. On the other hand, the physical and chemical properties of ScB_xRh_3 and CeB_xRh_3 vary with the concentration of boron on *B*-sites although the atomic ratio of the atoms on *A*-site to Rh atoms is fixed at 1:3. In these systems, the lattice constants increase with boron concentration. In this report, it is studied whether the change of the lattice constant influences the charge of the atoms on *A*-site, although the atoms on *A*- and *B*-sites are not directly bonded.

2. Experimental

Polycrystalline samples of $ScBRh_3$–$ScBRh_3$ and $CeBRh_3$–$CeRh_3$ systems were synthesized by the arc

*Corresponding author. Fax: +81-22-215-2132.
E-mail address: oku@imr.tohoku.ac.jp (M. Oku).

0022-4596/$ - see front matter © 2003 Elsevier Inc. All rights reserved.
doi:10.1016/j.jssc.2003.03.001

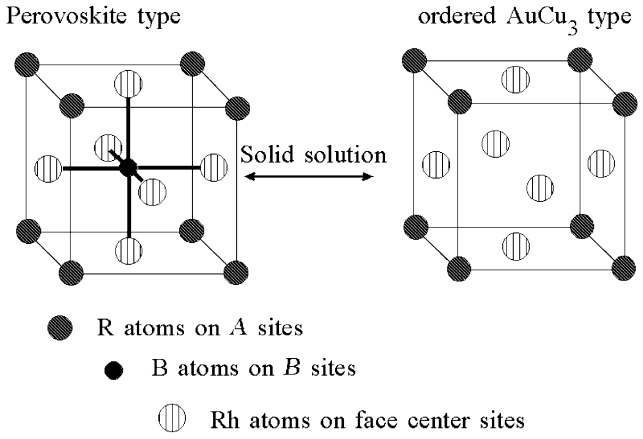

Fig. 1. Schematic crystal structures of perovskite type RB_xT_3(R=Sc, Ce, T=Rh) and ordered $AuCu_3$ type RT_3.

melting method using 99.9% pure Sc, Ce, Rh and B as raw materials. These were weighted with respect to their atomic ratios. The mixture of the starting materials, about 2 g for each sample, was placed in a water-cooled copper hearth in a reaction chamber. Argon was used as a protective atmosphere. The residual oxygen in the argon gas was eliminated by fusing a button of titanium as a reducing agent. The starting materials were then melted for 3 min by an argon arc plasma flame with a dc power source at 20 V and 100 A. The samples were then turned over and melted three times under the same conditions. Finally the synthesized samples were wrapped with tantalum foil and annealed at 1573 K for 20 h under to ensure homogeneity. The samples for chemical analysis were fused with a flux reagent of $NaHSO_4$, and then the resulting materials were dissolved into HCl. The chemical composition of each solution was determined by the induction coupled plasma atomic emission spectrometry (ICP-AES) method, in which Zn was used as an internal standard. The X-ray diffraction patterns showed that all the samples have a single phase of the space group $Pm\bar{3}m$.

All XPS spectra were obtained using an SSX-ES 100 electron spectrometer, which has a monochromatic Al$K\alpha$ X-ray as its primary excitation source. Its background pressure was less than 1×10^{-7} Pa. All spectral binding energies were referenced to the Fermi level. A 300-mm spot X-ray size and an angle-integrated mode were used to acquire all spectra reported in this work. The FWHM of Au $4f_{7/2}$ peak at 83.95 ± 0.02 eV is 1.03 eV. The samples for the XPS measurements were fixed with a vacuum compatible conductive resin in copper holders. They were fractured in the spectrometer in situ. XPS were taken more than two times for each boride sample having same chemical compositions, and good reproducibilities were obtained without contaminated signals.

NMR measurements were carried out with a conventional phase coherent pulsed NMR spectrometer under a magnetic field of about 6 T. The Knight shifts of ^{45}Sc were obtained from power spectra of fast Fourier transform (FFT) of free-induction decay as a function of frequency. As reference for Sc, $\gamma_{Sc}=10.343$ MHz/T is used.

3. Results and discussion

The dependence of the lattice constant of $ScBRh_3$–$ScRh_3$ and $CeBRh_3$–$CeRh_3$ systems on the boron concentration is shown in Fig. 2. The dependence of $CeBPd_3$–$CePd_3$ system [6] is compared in order to discuss the electronic structure of CeB_xRh_3. The lattice constant increases with the concentration of boron for both systems. The atomic distances between Sc and Rh, and Ce and Rh in $ScRh_3$, $ScBRh_3$, $CeRh_3$ and $CeBRh_3$ are 92%, 96%, 90% and 93% of the sum of the elements' radii, respectively, where the elements' radii are cited from Ref. [7].

The atomic distance between A and B atoms having covalent bonding is influenced by the difference of their electronegativities as suggested by Schomaker and Stevenson [8].

The correction for the atomic distance between A and B atoms in a solid due to the difference of the electronegativity is $-0.009\ |\chi_A-\chi_B|$ nm. The corrections for Sc–Rh and Ce–Rh are 0.008 and 0.009 nm, respectively. These corrections are too small to explain the atomic distances for the Sc–Rh and Ce–Rh of RB_xRh_3 systems. It means that the hybridization of orbitals between Sc, Ce and Rh shortens the atomic distance.

Fig. 3 shows Sc $2p_{3/2}$ XPS for the ScB_xRh_3 system. The spectral profiles of Sc $2p_{3/2}$ for ScB_xRh_3 are represented with a symmetrical Gaussian peak, but

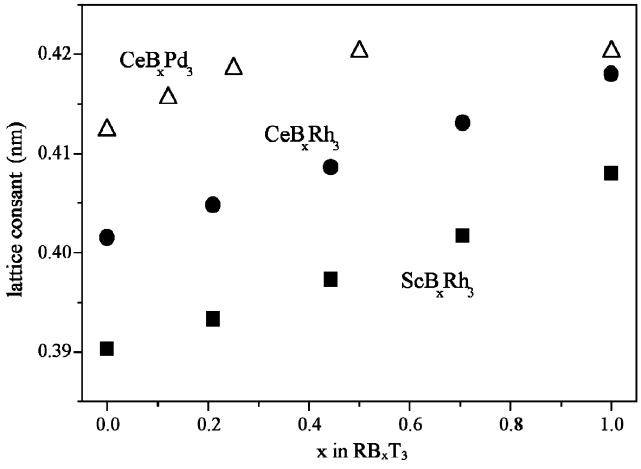

Fig. 2. Dependence of lattice constant of RB_xT_3 (R=Sc, Ce, T=Rh, Pd) on boron content x The errors of the lattice constants are under 0.05 nm. CeB_xPd_3: referred from Ref. [6].

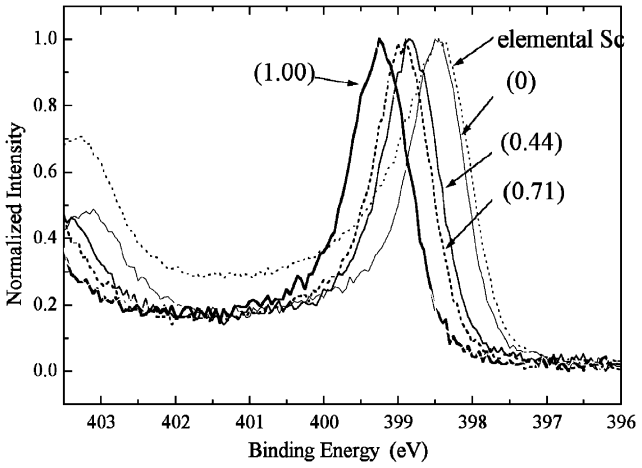

Fig. 3. Sc $2p_{3/2}$ XPS for ScB_xRh_3 and elemental Sc.

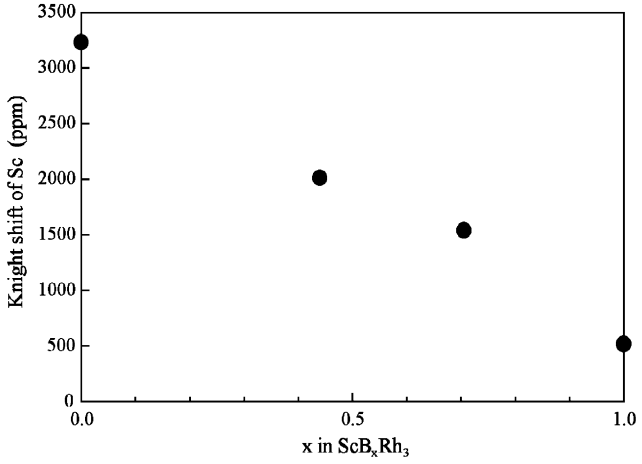

Fig. 4. Dependence of Knight shift of ^{45}Sc for ScB_xRh_3 on boron x. The relative errors of the shift are under 1%.

elemental Sc has an asymmetrical peaks. Moreover, FWHMs for ScB_xRh_3 are smaller than that for the element, and they do not change over all the boron concentration. The Sc $2p_{3/2}$ binding energy of 398.45 eV for $ScRh_3$ is slightly higher than 398.38 eV for elemental Sc, and it increases with the boron content. The intensity of Sc LVV Auger electrons was too weak to obtain good spectra having large signal-to-noise ratio, where the long accumulations of photoelectrons caused change of the surface state.

The temperature dependence of the ^{45}Sc Knight shift for $ScRh_3$ has been measured between 10 K and room temperature. It changes from 0.360% (10 K) to 0.318% (room temperature) as temperature changed. The temperature dependence of the Knight shifts in the other samples was smaller than 0.01%. The Knight shift of ^{45}Sc decreased with x in $ScRh_3B_x$ as shown in Fig. 4.

The ab initio calculations for $ScRh_3$ and $ScBRh_3$ have been reported by us [9] The results of the calculation regarding to Sc orbitals are the following. Comparing with the elemental Sc, the Sc 3d, 4s, and 4p orbitals for $ScRh_3$ are located at the inner sides of the Fermi levels. The PDOS of the levels have continuously some values from the valence to the conduction bands. The PDOS of Sc 3d and Sc 4s at the Fermi level drop into one tenth from $ScRh_3$ to $ScBRh_3$. Using geometrical partitioning of charge (i.e., Wigner Seitz cell partitioning), we found that relative to $ScRh_3$, in $ScRh_3B$, 0.5 electrons per Sc atom in the unit cell are lost and 0.08 electrons per Rh atom in the unit cell are gained.

The binding energy of core level depends not only on charge of the atoms but also on surrounding atoms. It is caused by an extra relaxation effect after photoemission of the core electron. The lack of good Sc Auger electron spectra for the system of ScB_xRh_3 prohibits us from the quantitative discussion of the chemical shift of Sc levels. However, we can say the following from the Sc 2p XPS. FWFM of Sc $2p_{3/2}$ in the system of ScB_xRh_3 did not depend on the concentration. It indicates that the charge on Sc atoms has a unique value and for each x, irrespective of whether the nearest B-sites are occupied or empty. In other words, the compounds of ScB_xRh_3 ($0<x<1$) are not a mixture of $ScRh_3$ and $ScBRh_3$ even in the life time of XPS. Although the Knight shift of ^{45}Sc is reflected from the Sc 4s electron state, the unique charge of Sc atoms is supported by the linear dependence of the Knight shift of ^{45}Sc with the boron concentration. The increase of the positive charge from $ScRh_3$ to $ScBRh_3$ was obtained from the ab initio band calculation. Then it is thought that the binding energy of Sc $2p_{3/2}$ increases with the increase of the positive charge in the system of ScB_xRh_3. Such dependence of the metal core levels have been well known in many metal–oxygen systems.

The curve fitting results of Ce 3d XPS for $CeRh_3$ and $CeBRh_3$ are shown in Fig. 5. The constraints for the curve fitting with Shirley type background subtraction

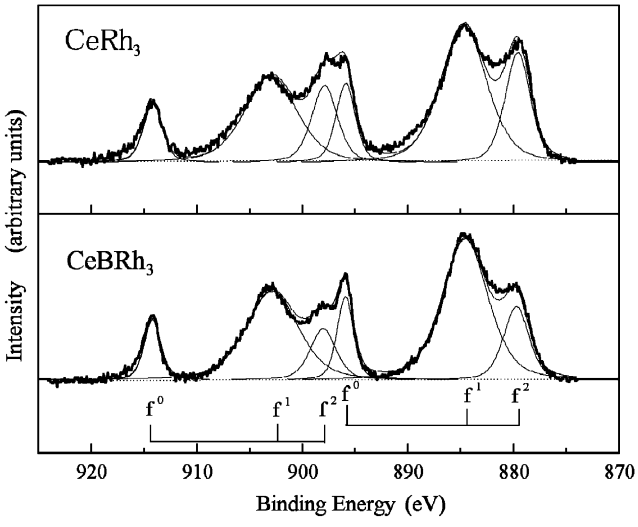

Fig. 5. Curve fitting of Ce 3d XPS for $CeRh_3$ and $CeBRh_3$.

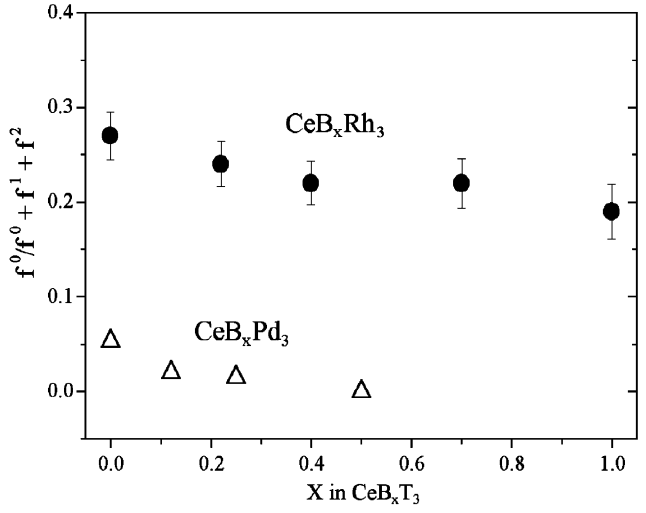

Fig. 6. Dependence of f^0 intensity on boron content in CeB_xRh_3 and CeB_xPd_3 CeB_xPd_3: referred from Ref. [14].

are follows: The spin–orbit splitting is same for the final states of f^0, f^1 and f^2. The intensity ratio of $3d_{5/2}-3d_{3/2}$ for each final state is the statistical ratio of Ce $3d$ level. Braicovich et al reported Ce $3d$ XPS excited with Mg and Al$K\alpha$ X-ray for $CeRh_3$ scraped with a diamond file [10]. Owing to the large photoelectron kinetic energy, they considered that the Al$K\alpha$ excited photoelectron spectrum is a good approximation to the bulk. However, their intensity of f^0 is lower than that in Fig. 5. The difference may originate from the surface preparation methods, where scraping the sample increases the surface contribution. The long exposure of the sample to the atmosphere of the spectrometer changed the spectral profile into a different profile, in which f^0 peak of $3d_{5/2}$ was not well separated from f^2 peak of $3d_{3/2}$. The change is explained with the sample oxidation by the residual gases in the spectrometer.

In the system of CeB_xPd_3 [10], there are three final states after Ce $3d$ photoemission when x is zero. The intensity of f^0 decreases with increase of x, and vanishes at $x = 0.5$ as shown in Fig. 6. This means that Ce in $CePd_3$ is in mixed valent state. The absence of f^0 peak in $CeB_{0.5}Pd_3$ and $CeSn_3$ [11] is explained by the fact that the Ce–Ce atomic distance is too large to interact with each Ce atoms. In the CeB_xRh_3 system, although the intensity of f^0 decreases with increase of x, the peak is observed even at x of one. The spectrum indicates that Ce in $CeBRh_3$ is still in a mixed valent state. The number of f electrons in $CeRh_3$ and $CeBRh_3$ are 0.6 and 0.7, respectively. The values are calculated with constant □ of 0.38 eV by a theory of Fuggle et al. [12] The lattice constant of $CeBRh_3$ corresponds to that $CeB_{0.2}Pd_3$ as shown in Fig. 2. The f^0 intensity for the former is larger than that for the latter. This indicates that the transition metal plays an important role in correlation between Ce–Ce atoms in CeB_xT_3 systems.

4. Conclusion

The core level XPS of rare earth atoms for ScB_xRh_3 and CeB_xRh_3 and ^{45}Sc NMR spectra show that their electronic structures change with boron concentration. It has been considered in perovskite oxides that the interaction between *A*- and *B*-site atoms are negligibly small. The addition of boron atoms in RRh_3 (R = Sc and Ce) having $AuCu_3$ type structure increases the lattice constant, and makes perovskite type borides. In these systems, although boron atoms are not directly bonded to rare earth atoms, the valence state of rare earth atoms changes with boron content.

Acknowledgments

The XPS and NMR measurements discussed of this work were performed at the Laboratory for Developmental Research for Materials, Institute for Materials Research (IMR), Tohoku University.

References

[1] T. Shishido, J. Ye, S. Okada, T. Sasaki, S. Osida, T. Naka, M. Oku, I. Higashi, K. Kishi, H. Horiuchi, T. Fukuda, J. Alloys Compds. 309 (2000) 107–112.
[2] T. Shishido, J. Ye, K. Kudou, S. Okada, M. Oku, K. Iizumi, M. Tanaka, S. Kohiki, Y. Kawazoe, K. Nakajima, unpublished.
[3] S.A. Barret, A.J. Jacobson, B.C. Tofield, B.E. Fender, Acta. Crystallogr. B 38 (1982) 2775–2781.
[4] J.A.M. Van Roosmalen, E.H.P. Cordfunke, R.B. Helmholzt, J. Solid State Chem. 110 (1994) 100–105.
[5] A.R. Chakhmouradian, R.H. Mitchell, P.C. Burns, J. Alloys Compd. 307 (2000) 149–156.
[6] S.K. Dhar, S.K. Malik, R. Vijayahavan, Phys. Rev. B 24 (1981) 6182–6184;
S.K. Dhar, S.K. Malik, R. Vijayahavan, Mater. Res. Bull. 16 (1981) 1577.
[7] F.D. Bloss, Crystallography and Crystal Chemistry, Mineralogical Society of America, Washington, DC, 1994, p. 206.
[8] V. Schomaker, D.P. Stevenson, J. Am. Chem. Soc. 63 (1941) 37–40.
[9] M. Oku, T. Shinohara, Q. Sun, Y. Kawazoe, K. Wagatsuma, T. Shishido, J. Alloys Compds. 339 (2002) 317–326.
[10] L. Braicovich, L. Duo, P. Vavassori, G.L. Olcese, Surf. Sci. 331–333 (1995) 782–786;
L. Duo, P. Vavassori, L. Braicovich, N. Witkowski, D. Malterre, M. Grioni, Y. Baer, G.L. Olcese, Z. Phys. B 103 (1997) 63–67.
[11] E. Wuilloud, W.-D. Schneider, B. Delley, Y. Baer, F. Hulliger, J. Phys. C: Solid Phys. 17 (1984) 4799–4806.
[12] J.C. Fuggle, F.U. Hillbrecht, Z. Zolnierek, R. Läesser, Ch. Freiburg, O. Gunnarsson, K. Schonnhammer, Phys. Rev. B 27 (1983) 7330–7341.